View metadata, citation and similar papers at core.ac.uk
brought to you by CORE
provided by Repositorio Institucional de la Universidad de Alicante

Glutamate adsorption on the Au(111) surface at different pH values

José M. Gisbert-González[a], *William Cheuquepán*[a,c], *Adolfo Ferre-Vilaplana*[b], *Enrique Herrero*[a]*, *Juan M. Feliu*[a]

[a]Instituto de Electroquímica, Universidad de Alicante, Apdo. 99, E-03080 Alicante, Spain.

[b]Instituto Tecnológico de Informática, Ciudad Politécnica de la Innovación, Camino de Vera s/n, E-46022 Valencia, Spain, and Departamento de Sistemas Informáticos y Computación, Escuela Politécnica Superior de Alcoy, Universidad Politécnica de Valencia, Plaza Ferrándiz y Carbonell s/n, E-03801 Alcoy, Spain.

[c]Present address. Facultad de Ciencias, Departamento de Química, Pza. Misael Bañuelos s/n, 09001 Burgos, Spain

* Corresponding Author, e-mail: herrero@ua.es

Abstract

Adsorbed amino acids can modulate the behavior of metal nanoparticles in advanced applications. Using a combination of electrochemical experiments, FTIR spectroscopy, and DFT calculations, glutamate species interacting with the Au(111) surface in solution are here investigated. Electrochemical results indicate that the adsorption behavior depends on the solution pH (which controls the glutamate ionization) and on the charge of the surface. Glutamate adsorption starts at potentials slightly negative to the potential of zero charge. The thermodynamic analysis of these results indicates that two electrons are exchanged per molecule, implying that both carboxylic groups become deprotonated upon adsorption. The FTIR spectra reveal that carboxylate groups are bonded to the surface in a bidentate configuration (with both oxygen atoms attached to the surface). Plausible adsorbed configurations, consistent with the whole of these insights, were found using DFT. Moreover, it was observed that glutamate oxidation only takes place when the surface is oxidized, which suggests that this oxidation process involves the transfer of an oxygen group to the molecule, though, according to the FTIR spectra, the main chain remains intact.

1. Introduction.

Molecules adsorbed on the surfaces of metal nanoparticles (NPs), acting as shapers, stabilizers, biocompatibilizers, or functionalizers, are in the core of advanced applications of these components in nanomedicine, bionanotechnology, nanosensors, or pharmaceutical compounding [1-3]**Error! Bookmark not defined.**. Being the building block of proteins, the biocompatibility of amino acids is guaranteed. Thus, amino acids as adsorbed agents are a natural choice for these applications. Additionally, the wide number of different functional groups in the amino acids provides numerous opportunities to tailor the properties of the ensembles for the application. Amino acids have been used as linkers between drugs and nanoparticles, enabling target delivery [1, 2], and they have been used to immobilize biomolecules on electrodes in biosensors [3, 4]. Platinum and, mainly, gold, also because of its biocompatibility, are among the most investigated metals for these applications [5, 6]. Therefore, a deep knowledge of the interaction mechanisms of amino acids with those metals in solution is essential for the optimization of these applications.

Amino acid-metal interactions have been investigated in the last decades [7], though the interaction mechanisms have not been completely elucidated yet. On one hand, given that an adsorbent-adsorbate interaction depends on the specific arrangement of the surface atoms, fundamental studies require well-defined surfaces. In fact, studies of glycine [8-12], L-alanine [13-16], and L-serine [14-19] on single-crystal platinum and gold indicate that amino acid-metal interactions depend not only on the surface geometry but also on the solution pH, suggesting that these species adsorb preferentially through carboxylic groups, although in some cases, adsorption through the amino moiety has also been observed. On the other hand, combined techniques are often required to have a full

description of the interaction. For instance, electrochemical experiments can identify hydrogenation states, but they cannot determine the geometry, and spectroscopic experiments can provide evidence of the presence of some functional groups, but they cannot unequivocally determine geometry either. However, theoretical DFT calculations can give rise to plausible adsorbent-adsorbate configurations consistent with electrochemical and spectroscopic experiments, so that a reasonably confident description of the interaction can be obtained. We have recently applied such a kind of combined approach to citrate interacting with platinum and gold [20, 21], unraveling the growing mechanism of NPs with preferential shape.

Being similar to citric acid, L-glutamic (Glu) acid interacting with the Au(111) surface is here investigated using a combination of electrochemical experiments as well as the usage of ATR-SEIRAS spectroscopy and DFT calculations. More complex derivatives of this amino acid, such as the poly-γ–glutamic acid, have been already used as adsorbed agents in nanomedical applications [22, 23]. Both citric acid and Glu present a main chain formed by two terminal carboxylic groups separated by 3 carbon atoms, differing only in the side groups. Citric acid presents a carboxylic and an OH group in the β position, whereas Glu has an amino group in the α carbon. Thus, Glu contains three acid/base groups, whose pK_a values are 2.17, 4.25, and 9.67. Therefore, the main form in aqueous solutions will be different depending on the pH value, which can affect the surface interaction. For this reason, the interaction at different pH values is investigated.

2. Methods

2.1. Experimental methods

Au(111) single crystal electrodes were prepared according to Clavilier's method [24, 25]. Ultrapure 0.5 mm diameter gold wire was fused and crystallized, to obtain a single

crystal bead. The bead was mounted in a four-cycle goniometer on an optical bench, oriented using a laser reflection, and cut and polished with diamond paste until mirror finishing.

For the internal reflection infrared spectroscopy experiments (ATR-SEIRAS), the working electrode was prepared from a 25 nm-thick gold thin film (Au(111)-25nm) (99.999%, Kurt J. Lesker Ltd.) thermally evaporated on the (111) orientation on a low oxygen-content silicon prism beveled at 60º (Paster Ltd, Japan). The deposition was accomplished in a PVD75 vacuum chamber (Kurt J. Lesker Ltd.) coating system at a base pressure of about 10^{-6} Torr. Both the gold-film thickness and the deposition rate (0.006 nm s^{-1}) was controlled by using a quartz crystal microbalance. Once the electrode was set up on the spectroelectrochemical cell, it was cleaned and electrochemical annealed by cycling the electrode potential at 20 $mV \cdot s^{-1}$ between 0.05 and 1.1 V for 1 h (sodium acetate was added up to a 10 mM concentration) Subsequently, the spectroelectrochemical cell was thoroughly flushed with a 0.1 M $HClO_4$ until acetate anions were removed. Based on the preferential (111) orientation of the samples obtained with this procedure, the Au(111)-25 nm notation is adopted in this work [26].

All the electrochemical experiments were conducted in a glass cell using a reversible hydrogen electrode (RHE) for pH=1 and pH=13 solutions and an Ag/AgCl (1 M KCl) electrode (subsequently transformed to the RHE for data comparison) for pH=3 and pH=5 as reference electrodes. A gold wire was used as counter-electrode. The working solution was prepared using L(+)-glutamic acid (Glu) (99% ACROS ORGANICS), concentrated perchloric acid (Merck Suprapur®), and ultrapure water (18.2 MΩ·cm, TOC 50 ppb max, Elga Vivendi). For alkaline solutions, sodium hydroxide monohydrate (Merck Suprapur®) was used. Buffer solutions were also prepared for some experiments to maintain the pH constant through the addition of glutamate using sodium

fluoride (Merck Suprapur®). In some experiments, the working solution was prepared in deuterium oxide (99% D_2O, Aldrich). All solutions were deaerated with Ar (N50, Air Liquide). Voltammetric experiments were carried out using a wave signal generator (EG&G PARC 175), potentiostat (eDAQ 161), and digital recorder (eDAQ e-corder 401) workstation. All experiments were carried out at room temperature.

2.2. Computational methods

All DFT calculations were carried out using numerical basis sets [27], semi-core pseudopotentials [28] (which include scalar relativistic effects), and the revised Perdew-Burke-Ernzerhof (RPBE) [29] functional as implemented in the Dmol^3 code [30]. Dispersion forces were corrected by the Tkatchenko and Scheffler method [31]. Continuous solvation effects were taken into account by the conductor-like screening model (COSMO)[32]. The effects of non-zero dipole moments, in the supercells, were canceled using external fields [33]. Proton-coupled electrons transfers were modeled employing the computational hydrogen electrode formalism [34].

The Au(111) surface was modeled using a big and thick enough periodic supercell as for modeling chemisorbed glutamate species with and without the amino group protonated under neutral total charge conditions. The model comprises 72 Au atoms (six layers of metal atoms) and a vacuum slab of 20 Å. The most internal 24 Au atoms (two layers of metal atoms) were frozen in their bulk crystal locations, meanwhile, the remaining more external 48 Au atoms were completely relaxed jointly with the adsorbates. The shortest distance between periodic images was in the order of 8.34 Å.

Optimal adsorbent/adsorbate configurations were searched for using numerical basis sets of double-numerical quality. For this phase of the calculations, the optimization convergence thresholds were set to 2.0×10^{-5} Ha for the energy, 0.004 Ha/Å for the force,

and 0.005 Å for the displacement. The SCF convergence criterion was set to 1.0×10^{-5} Ha for the energy. Assuming the previously optimized configurations, energies were estimated using numerical basis sets of double-numerical quality plus polarization. In this case, the Self Consisted Field (SCF) convergence criterion was set to 1.0×10^{-6} Ha for the energy.

Orbital cutoff radius of 3.1, 3.7, 3.3, and 4.5 Å were always used in the numerical basis set for H, C, O, and Au atoms, respectively. Brillouin zones were always sampled, under the Monkhorst-Pack method using grids corresponding to distances in the reciprocal space of the order of 0.04 1/Å. Convergence was always facilitated introducing 0.002 Ha of thermal smearing, though total energies were extrapolated to 0 K. The value 78.54 was taken as the dielectric constant for water in the continuous solvation model.

3. Results and discussions

3.1. Voltammetric behavior

Given that Glu presents several acid/base groups, with significantly different pK_a values (2.17 for the carboxylic group close to the amino group, 4.25 for the second carboxylic group, and 9.67 for the amino group), the dominant glutamate species interacting with the surface can depend on the solution pH. Thus, four glutamate species can be found in solution, whose ionization are pH-dependent. At pH<2.17, the amino group is protonated, forming a cation. Between 2.17 and 4.25, the deprotonation of the α-carboxyl group gives rise to a neutral zwitterion, with the amino group still protonated. Between 4.25 and 9.67, the second carboxylic group becomes deprotonated, yielding an anion with a -1 charge. Finally, at pH> 9.67, the amino group loses the acidic proton, becoming a double negative anion. For this reason, the adsorption behavior of glutamate species on the Au(111) electrode was studied using solutions with pHs 1, 3, 5, and 13,

each value inside a different region of stability of the species. The electrolytes used to prepare the solutions should fulfill two requirements: enough buffer capacity, to avoid pH changes, and absence of specific adsorption so that the interaction of glutamate species can be studied without interferences. The prepared solutions were 0.1 M $HClO_4$ (nominal pH=1), 2.99×10^{-2} M $HClO_4$ + 4.84×10^{-2} NaF (pH=3), 1.70×10^{-6} M $HClO_4$ + 10^{-3} M NaF (pH=5) and 0.1 NaOH (pH=13). Being HF a weak acid with pK_a=3.15, the combination of $HClO_4$ and NaF gives rise to the formation of HF/F^- buffered solutions, which are able to maintain the solution pH while the glutamic acid concentration is increased. Besides, no specific adsorption takes place in these buffer solutions, because the interactions between the HF/F^- pair and the gold surface are weak and compete with those of the ClO_4^- anions for compensating the increase in the positive charge density on the electrode surface as the potential is made more positive.

The voltammetric study is divided into two regions, the so-called double layer region (E<1.2 V) and the OH adsorption and oxidation region (E>1.2 V) [35-37]. In the double-layer region, the behavior under acidic conditions (pHs 1, 3, and 5) is different from that observed in alkaline media [38, 39]. Under acidic conditions and in the absence of Glu, the voltammetric profile is almost featureless (Figure 1). In spite of that, it should be noted that the behavior of the Au(111) surface is complex. After annealing, the surface is reconstructed, displaying a $(22\times\sqrt{3})$ structure (also termed as herringbone structure) [40, 41] and, when the electrode is immersed in the solution at low potentials (close to 0 V in the RHE scale), this reconstruction is maintained. When the electrode potential is increased, the reconstruction is lifted and a nominal (1×1) structure is obtained [42]. The transition between both structures is triggered by the charge [43], so that a positive surface charge induces the lifting of the reconstruction, whereas negative values cause the progressive formation of a reconstructed surface. The kinetics of these transition

processes between both structures are slow, but, in general, the lifting of the reconstruction is significantly faster than the reconstruction process [44]. Due to this slow kinetics, two different potentials of zero charge (pzc) for the unreconstructed (pzc_u) and the reconstructed (pzc_r) surface can be measured (as shown in Figure 1). Both values are pH-independent in the SHE scale. For low electrolyte concentrations, and according to the Stern model of the double layer, the pzc is located in the minimum of the capacity curve[45], which translates to a minimum in current in the voltammetric profile. As the negative-swept does not experience a fast surface-reconstruction phenomenon, the minimum in the voltammetric profile allows a fast estimation of the pzc when low concentration electrolyte solutions are used. However, in this case, the slow kinetics of the surface reconstruction processes results in an asymmetrical profile with respect to the current axis. The voltammetric profiles show, also in this case, some features that can be related to the non-specific anion adsorption on the surface, which obviously, depends on the surface state. As expected, those non-specific anions adsorption processes take place at potentials higher than the pzc, and shift to higher potential values in the RHE scale as the pH increases. Despite the complexity of the profile, at pH=3, a small local minimum can be observed in the negative scan direction. This minimum is more clearly resolved at pH=5 because the total electrolyte concentration is lower. The position of the minima coincides with the measured values of the pzc_u using capacitance measurements [45-47], which indicates that the surface at those potentials in the negative scan direction is still unreconstructed. In the positive scan direction, the minima cannot be observed, probably because of the overlapping of the minimum related to the pzc_r with the signal corresponding to the adsorption of OH or electrolyte anions.

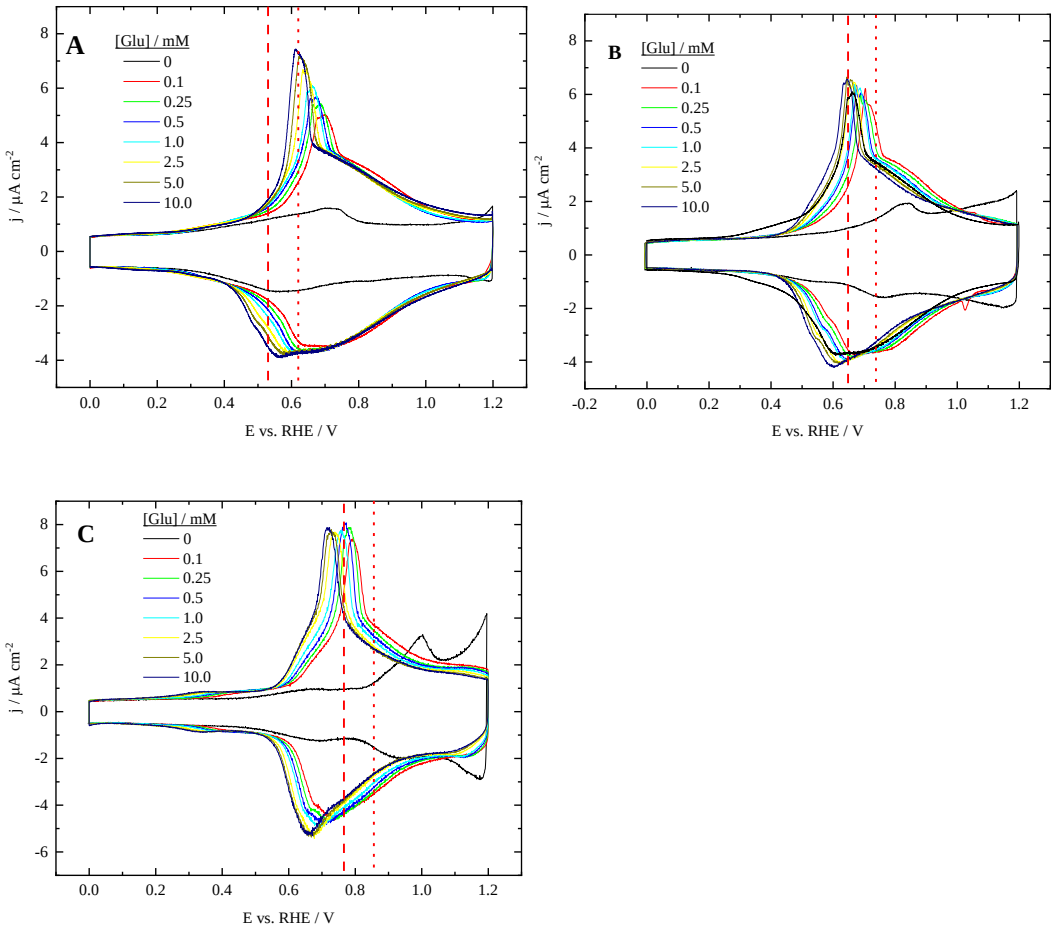

Figure 1. Voltammetric profiles of the Au(111) electrode after the addition of different Glu concentrations in A) 0.1 M $HClO_4$ (pH=1); B) 2.99×10^{-2} M $HClO_4$ + 4.84×10^{-2} NaF (pH=3) and C) 1.70×10^{-6} M $HClO_4$ + 10^{-3} M NaF (pH=5). Scan rate: 20 mV s^{-1}. The vertical lines mark the position of the pzc_u (dashed line) and pzc_r (dotted line) of the Au(111) surface.

After the addition of Glu, even in low concentrations, the voltammetric profiles of the Au(111) electrode show significant changes when compared to those obtained in its absence in acidic media. The addition of Glu results in a complex voltammetric profile, as a result of the interaction of glutamate with the Au(111) surface. The observed signals between 0.4 and 1.2 V are related to the specific adsorption of glutamate species on the surface. As expected, the signals shift to lower potential values as the total Glu concentration increases. In the positive scan direction, a sharp peak appears in the initial stages of the glutamate adsorption process. This peak is associated with the lifting of the reconstruction which is triggered by the surface charge [48, 49], implying that the surface charge at a constant potential for a given pH increases as the total Glu concentration in

solution increases. Apparently, the adsorption process of glutamate is completed at 1.2 V, which is the potential at which OH adsorption and surface oxidation processes take place on the unmodified surface.

On the negative scan direction, the desorption of the glutamate species accumulated on the surface occurs. In this case, only a complex wave without a significant peak is observed, indicating that the reconstruction is not taking place at a significant rate while glutamate is still adsorbed. The presence of adsorbed species usually stabilizes the (1×1) structure by lowering its surface energy [43]. In the second scan, the peak associated with the lifting of the reconstruction is always smaller than that recorded after flame annealing, a clear indication that the reconstruction process is slow (during the time elapsed in the potential region where glutamate species are not adsorbed, a fully reconstructed surface has not been achieved). It should be noted that the voltammetric profiles are symmetrical at potentials higher than the peak related to the lifting of the reconstruction in the positive scan (figure S1) (i.e., for E>0.65 V, E>0.68 V, and E>0.75 V for solutions containing 0.01 M Glu in pH=1, pH=3, and pH=5, respectively). This fact indicates that the adsorption process of glutamate species is fast and that the surface structure in this region is the same in the positive and negative scan directions.

The shift with pH of the signals related to glutamate adsorption can be used to determine the stoichiometry of the reaction, mainly, the ratio of the number of exchanged electrons to the number of protons involved in the adsorption process. For an accurate determination, the concentration of the main solution species should be kept constant and the analysis should be made in a pH range comprising several pH units. In this case, such a kind of accurate quantitative determination cannot be made for two reasons: i) the two first pK_a of Glu are relatively close and ii) there are not available buffered solutions for pH>5 in which the anions do not interact specifically with the surface. Despite that, a

qualitative analysis can be performed. Carboxylic acids are usually adsorbed through the carboxylate groups in a bidentate configuration in which both oxygen atoms are bonded to the surface. If the nature of the species and the atomic arrangement of the surface atoms allow it, the molecule can become attached to the surface by several carboxylate groups, as happens for instance for citrate [21], which can bond to (111) surfaces by the three carboxylate groups. Glu could be, simultaneously, attached by both carboxylate groups. In this case, the proposed reaction when $pH<pK_{a,1}$ is

$$\begin{aligned} &HOOC\text{-}\left(CH_2\right)_2\text{-}CH\left(NH_3^+\right)\text{-}COOH + 2Au \square \\ &\qquad Au\text{-}OOC\text{-}\left(CH_2\right)_2\text{-}CH\left(NH_3^+\right)\text{-}COO\text{-}Au + 2H^+ + 2e^- \end{aligned} \tag{1}$$

This adsorption process should move in the SHE scale 0.059 V per pH unit. For pH between 2.17 and 4.25, where the main species in solution is the zwitterion, the proposed reaction is:

$$\begin{aligned} &HOOC\text{-}\left(CH_2\right)_2\text{-}CH\left(NH_3^+\right)\text{-}COO^- + 2Au \square \\ &\qquad Au\text{-}OOC\text{-}\left(CH_2\right)_2\text{-}CH\left(NH_3^+\right)\text{-}COO\text{-}Au + H^+ + 2e^- \end{aligned} \tag{2}$$

with an expected change of 0.030 V per pH unit. Finally, in the pH range 4.25 to 9.67, the reaction is

$$\begin{aligned} &{}^-OOC\text{-}\left(CH_2\right)_2\text{-}CH\left(NH_3^+\right)\text{-}COO^- + 2Au \square \\ &\qquad Au\text{-}OOC\text{-}\left(CH_2\right)_2\text{-}CH\left(NH_3^+\right)\text{-}COO\text{-}Au + 2e^- \end{aligned} \tag{3}$$

This process should take place at constant potential in the SHE scale. To perform the analysis, the potential for the peak related to the lifting of the reconstruction for 0.001 M Glu will be used, because it takes place at a constant glutamate coverage. The peak position in the SHE scale is plotted in Figure 2. These points, which are in different regions, will be used to establish the trend lines (red lines in Figure 2) according to the proposed stoichiometry in each region. As can be seen, these lines intersect, within the error of the experiments, at the pK_a values, validating the proposed mechanism.

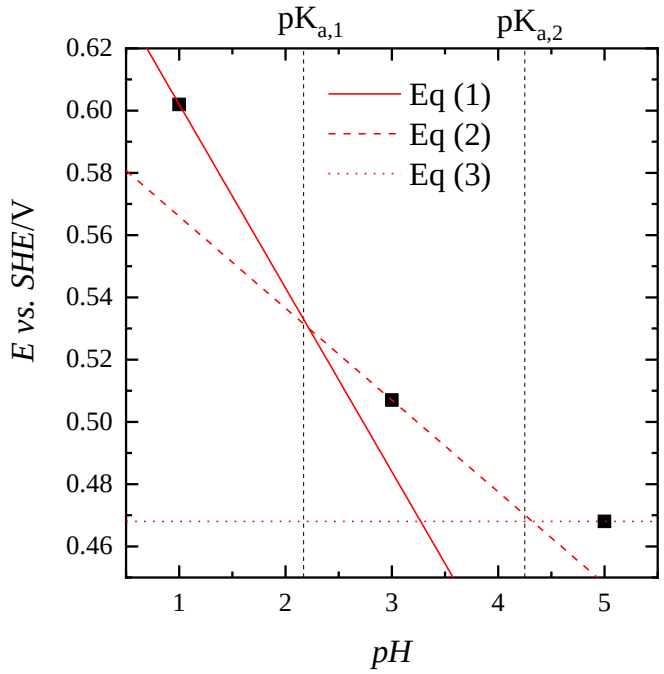

Figure 2. Potential, in the SHE scale, of the peak associated with the lifting of the reconstruction for [Glu]=0.001 M vs. pH. The red lines display the expected trends of the peak potential according to the different equations. The vertical lines mark the positions of the pK_a values.

Additional confirmation of the proposed stoichiometry can be obtained under alkaline conditions. As can be seen in Figure 3, in the absence of Glu, the peaks at 1.05 are related to OH adsorption [38, 39]. When Glu is added to the solution, the profile in the double-layer region is almost constant (E<1.0 V), and no additional processes are observed. This indicates that glutamate species are not adsorbed. This result is expected from the previously investigated potential dependence of the glutamate adsorption process. Under the proposed potential independent adsorption in the SHE scale for pH>$pK_{a,2}$, derived from the behavior in acidic solutions, glutamate species should not be adsorbed at pH=13, because the expected onset potential would be ca. 1.2 V. In fact, the surface presents a negative charge for this region at this pH, given that both pzc_u and pzc_r values are located at E>1.2 V vs. RHE. Owing to the high concentration of OH^- and its strong surface interaction, the adsorption of OH dominates over that of glutamate species, and this latter process cannot be observed. An additional feature of this voltammetric

behavior is that the oxidation process of Glu can be observed at potentials above 1.0 V. The process seems to be triggered by the adsorption of OH. In fact, the characteristic signals related to OH adsorption are still visible, especially for low Glu concentration. This observation clearly indicates that adsorbed OH is involved in the oxidation process.

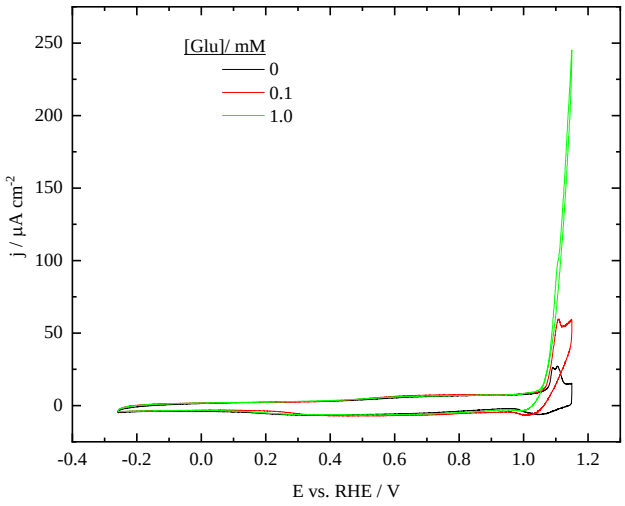

Figure 3. Voltammetric profile of the Au(111) electrode after the addition of different Glu concentrations in 0.1 M NaOH (pH=13). Scan rate: 20 mV s^{-1}.

From these results, it is clear that Glu can be oxidized at high potential values, coinciding with the oxidation of the gold surface. Figure 4A shows the voltammetric profiles of the Au(111) oxidation region at different acidic pH values in the presence and absence of Glu. When the solution is glutamate-free, two peaks can be perfectly distinguished. The first one corresponds to the transfer of one electron for the formation of a complete OH layer, whereas the second one corresponds to the transformation of this layer to the oxide Au-O layer[36]. There are small changes with pH, as reported previously, though the overall shape is maintained. The OH adsorption process is competitive with the weak adsorption processes of the other solution anions, such as ClO_4^- and F^-. The origin of the small changes is probably the concentration differences of the supporting electrolytes to maintain the buffer properties. It has been proposed that F^- is

more selectively adsorbed on the Au electrodes than ClO_4^- [48, 50], which can justify the small diminution of the OH adsorption peak at pH=5. Similar changes are observed for the peak related to the formation of the oxide layer. In the negative scan, the desorption of the Au-O layer takes place in a single peak (with a shoulder at low potentials), which is a clear indication that the formation of this oxide layer is irreversible. The overall shape of the voltammogram is maintained, and the differences in the shape can be explained by the differences in the solution properties.

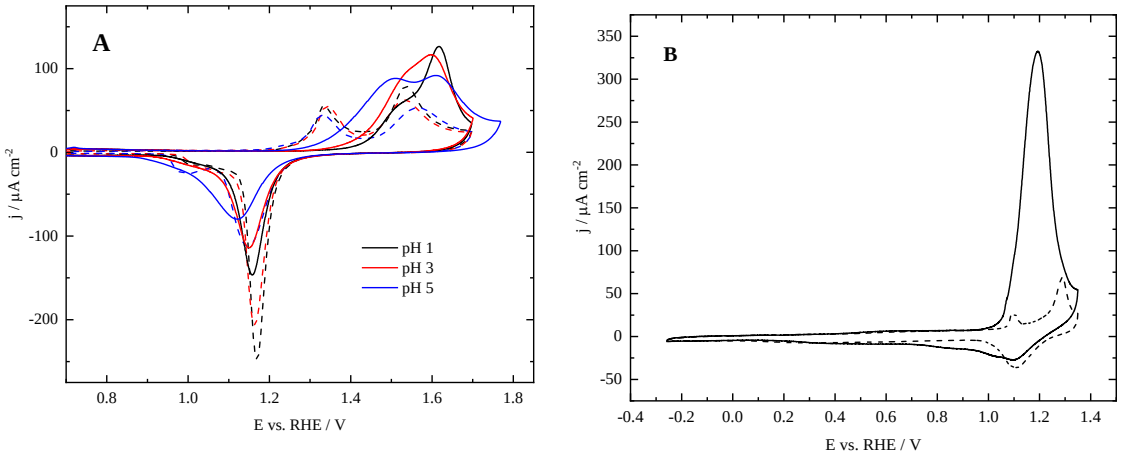

Figure 4. Voltammetric profiles for the Au(111) electrode in the oxide region in A) acidic values and B) alkaline solutions in the absence (dashed lines) and the presence of 0.001 M Glu (full line). Scan rate 20 mV s^{-1}.

Thus, when Glu is added, the onset for any process is displaced to more positive potentials, and the currents and the overall charge, under acidic conditions, are higher than those recorded in the absence of Glu in the positive scan direction. On the other hand, the reduction peak is significantly smaller. Both combined results indicate that glutamate species are being oxidized in this high potential region. Moreover, the oxidation process appears to be connected with the adsorption of OH. Additionally, as the pH increases, the onset shifts to lower potential values, and the overall charge related to this process increases. These differences can be related to the surface charge effect on the OH and glutamate species adsorptions. Fixed the potential in the RHE scale, as pH increases, the

surface charge becomes less positive. As a result, the glutamate species are less strongly adsorbed. However, the driving force for the OH adsorption process remains constant, given that the surface charge effect is counterbalanced by the OH^- concentration increase. Thus, for a given potential in the RHE scale, as the pH increases, the adsorption of OH becomes stronger in comparison with that of glutamate species, which favor the oxidation of glutamate in an OH mediated process. Another important consequence of the observed behavior is that the formation of the Au-O layer blocks the oxidation. As can be seen in Figure 4, the currents for the upper potential limit of the scan diminish significantly and no oxidation currents are observed in the negative scan direction. This behavior in acidic solutions is also confirmed under alkaline conditions (Figure 4B). In this case, since glutamate is not adsorbed, the onset of the oxidation coincides with the onset of OH adsorption. Moreover, the currents for the oxidation are significantly higher because the absence of a glutamate layer leads to an increase of the OH coverage at a constant potential in the RHE scale, which leads to higher currents.

To get additional insight into the role of adsorbed OH in the process, voltammetric scans with different upper potential limits were recorded and compared to the behavior obtained in the absence of Glu (Figure 5). At pH=5, the oxidation wave for Glu has two overlapping peaks, being the onset for the oxidation ca. 1.4 V (Figure 4A). In the absence of Glu, an OH layer is already adsorbed at these potentials, but the presence of the glutamate layer prevents the adsorption of OH. When the upper potential limit is 1.45 V (Figure 5A), oxidation currents, and a small hysteresis between the positive and negative scan directions are observed. When the upper potential is increased above 1.5 V, currents in the negative scan direction are almost negligible, indicating that a fast transformation of the surface is taking place. This behavior can be explained as follows. As the glutamate layer is desorbed and replaced by the OH layer, the surface behavior tends to approximate

that in the absence of Glu. At potentials above 1.4 V, the adsorbed OH layer is transformed into Au-O, which is inactive for the oxidation. This process is slow, and thus the oxide reduction peak in the negative scan direction contains less charge than in the absence of Glu. The behavior is even more clear at pH=13 (Figure 5B). At this pH value, the oxidation onset coincides with that of the OH adsorption. When the upper potential is set below 1.2 V (the potential at which the Au-O formation begins in the absence of Glu), significant oxidation currents can be recorded in the negative scan direction. Under these conditions, the OH reduction peak cannot be distinguished because it overlaps with large oxidation currents. For higher upper potentials, currents in the positive scan direction begin to diminish due to the progressive formation of the Au-O layer, which leads to small currents in the negative scan direction. As before, the presence of Glu delays the formation of Au-O because some OH species are being consumed in the glutamate oxidation reaction. For this reason, the reduction peak is smaller than that recorded for the same upper potential limit in the absence of Glu.

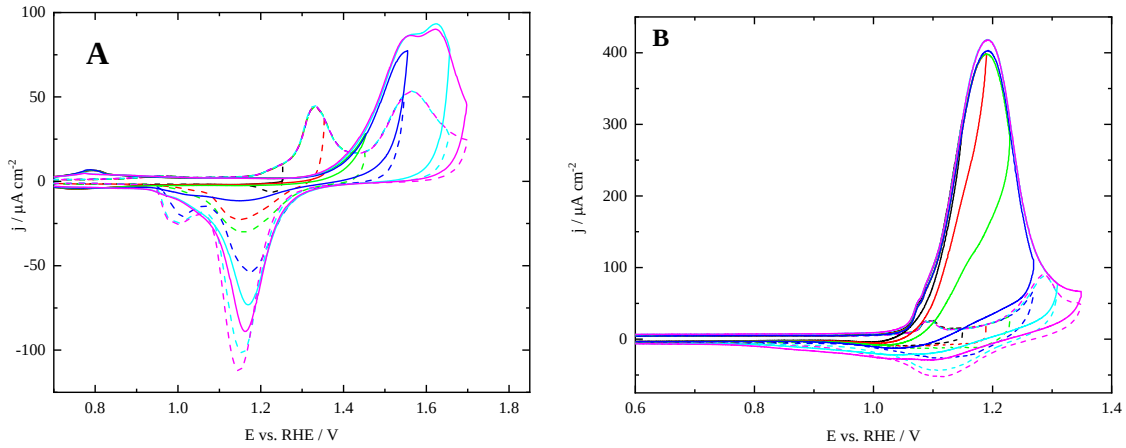

Figure 5. Voltammetric profiles for the oxide region of the Au(111) in A) pH=5 and B) pH=13 in the absence (dashed lines) and the presence of 0.001 M Glu (full line) with different upper potential limits. Scan rate 20 mV s^{-1}

3.1.1. Gibbs excesses

Additional information on the glutamate adsorption process can be obtained from the thermodynamic analysis of the obtained voltammetric results. The procedure has been already described [20, 21]. However, because of the surface reconstruction of gold, only the negative scan direction of the voltammograms is taken, given that the surface state must not change along with the studied processes. The excess determination begins with the integration of the profiles displayed in Figure 1, which correspond to glutamate desorption on the (1×1) surface following the procedure explained in reference [21]. In this way, potential vs. charge density curves can be obtained. To determine the surface charge, the integration constant has to be known and used as a reference. Since at the lowest potential, glutamate species are desorbed, the charge should be the same as in the supporting electrolyte. For this reason, zero is assigned as the nominal charge to the lower potential limit for all curves.

Charge vs. potential under acidic conditions is displayed in Figure 6. For pH=5 (Figure 6C), all the curves converge at the highest potential, a clear indication that the glutamate adlayer has been completed. However, for pHs 1 and 3, the curves do not converge. Different charge values at the upper limit can be due to one of two reasons: either the adlayer is not complete or a faradic process contributes to the measured charge. When the adsorption process has not been completed in the upper potential, a progressive convergence of all the curves should be observed when the potential approaches the upper limit. However, this is not the case, because the difference increases with potential, especially for the higher Glu concentrations, indicating that a faradaic process is contributing to the measured charge. This implies that glutamate species are being oxidized at a very low rate in the upper potential region, though the currents are too low

to be detected in a normal voltammetric scan. Moreover, this weak oxidation process is pH-dependent, given that, as pH increases, the total contribution of the oxidation process diminishes, because the difference in charge between the higher and lower Glu concentration diminishes, being negligible at pH=5. Under these conditions, the thermodynamic analysis can only be carried out for pH=5.

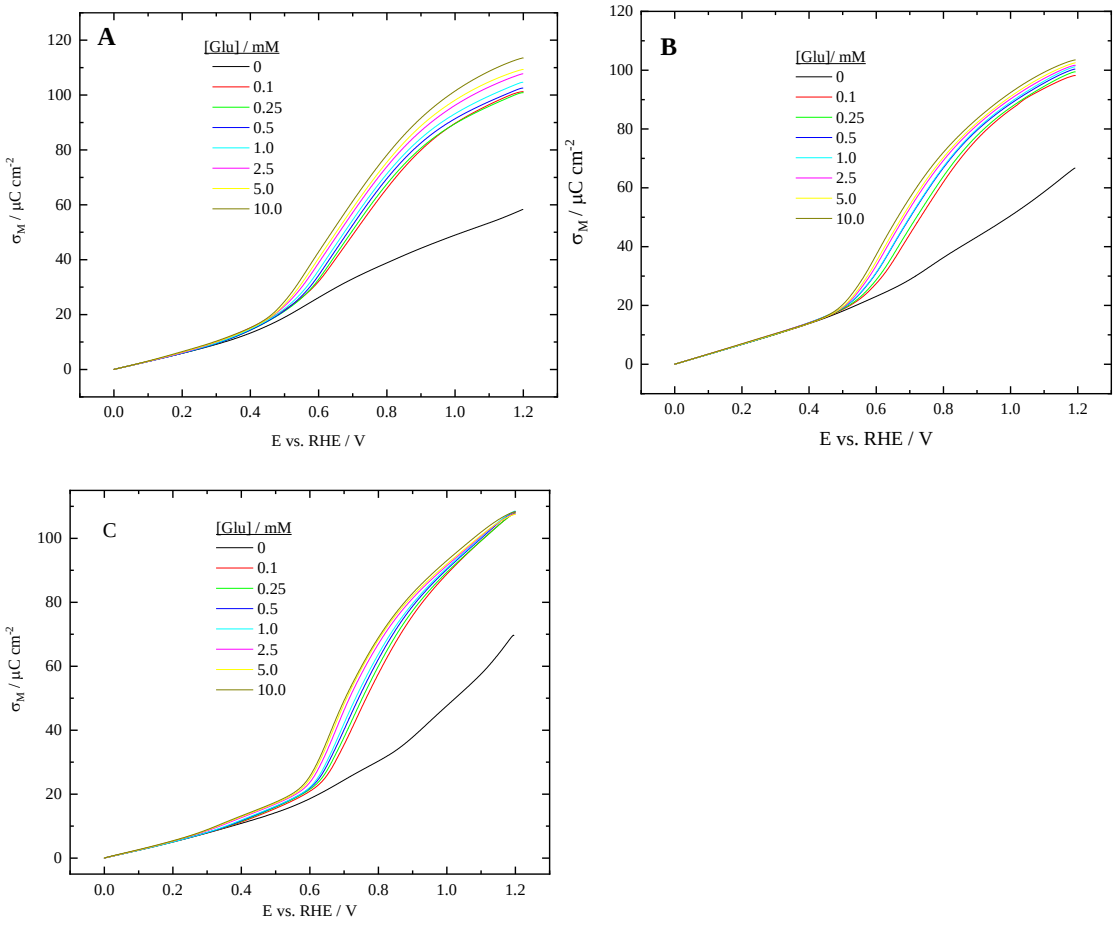

Figure 6. Charge vs. potential for the Au(111) electrode for different Glu concentrations in A) pH=1, B) pH=3 and C) pH=5.

Once the charge vs. potential curves have been obtained, surface excesses for glutamate species at pH=5 can be calculated using the procedure described in [21]. It should be stressed that the obtained values correspond to the total sum of the excesses of

all possible glutamate species. The curves (Figure 7) have the typical behavior observed for other anions. At this pH value, the adsorption onset is 0.3 V, meanwhile, the adlayer is completed at 1.2 V, where all curves for the different Glu concentrations merge. At this potential, the measured maximum excess is 2.7×10^{-14} ions cm^{-2}, which is equivalent to a surface coverage of 0.18. This value is very similar to that obtained for citrate [21]. Both citric acid and Glu have the main chain with two terminal carboxylic groups separated by three carbon atoms. Thus, if both molecules interact with the surface mainly through terminal carboxylate groups, adsorption energies and geometries will be very similar, and thus coverages should be also the same. On the other hand, Gibbs excesses seem to be quasi-independent from Glu concentration in the potential range $0.260 < E < 0.585$ V, which suggests that the surface-glutamate interaction at low coverages does not follow the typical behavior of adsorbed anions. This feature appears also when citrate is adsorbed on Au(111) [21, 51].

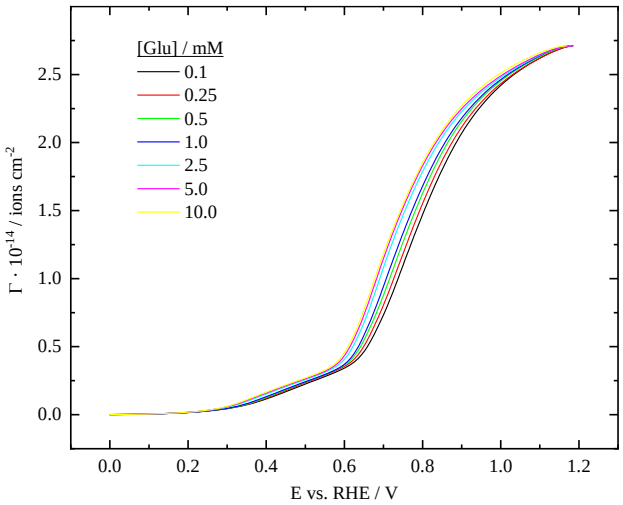

Figure 7. Gibb excesses vs. potential for the different Glu concentrations at pH=5.

Form surface excesses, charge transfer numbers for the adsorbed species can be calculated using the cross differential of the electrocapillary equation [52] according to

$$n' = -\frac{1}{F}\left(\frac{\partial\sigma}{\partial\Gamma}\right)_{\mu} = \frac{1}{F}\left(\frac{\partial\mu}{\partial E}\right)_{\sigma} = \frac{RT}{F}\left(\frac{\partial \ln c_{-}}{\partial E}\right)_{\sigma} \qquad (4)$$

where *n*' is the charge number at constant chemical potential, that is, the reciprocal of the Essin-Markov coefficient. The most reliable values can be obtained in the region where there is a large increase of the excesses with charge or concentration. Two electrons are transferred per molecule in the central potential region, where this latter condition is fulfilled, meanwhile, a higher number for lower and higher potentials is obtained. This result is consistent with the proposed reaction (3), implying that glutamate species can become attached to the surface through both carboxylate groups.

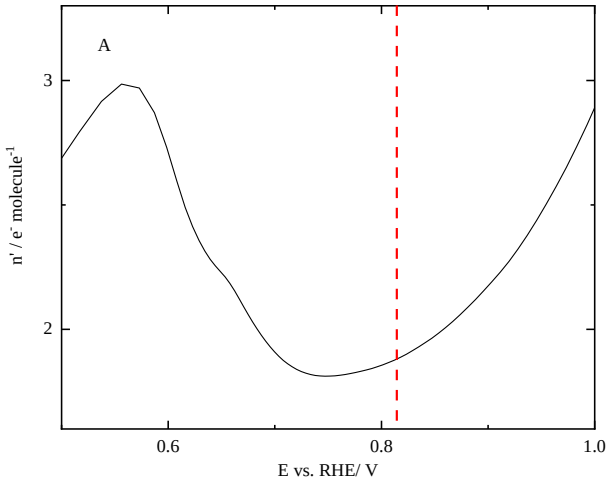

Figure 8. Charge number vs. applied potential at pH=5 for 10^{-3} M Glu

3.2. FTIR spectroscopy.

To identify the nature of the bonds involved in the glutamate adsorption on the Au(111) surface, FTIR experiments were conducted. Having advantages with respect to the external reflection mode, such as the minimal interference in the signal from bulk species and enhancement of the absorption due to the surface-enhanced infrared

absorption (SEIRA) effect, the attenuated total reflectance mode was used for this purpose. Under this mode, changes in the closest layers of the interphase to the electrode surface (solvent as well as other species) can be easily detected [53, 54].

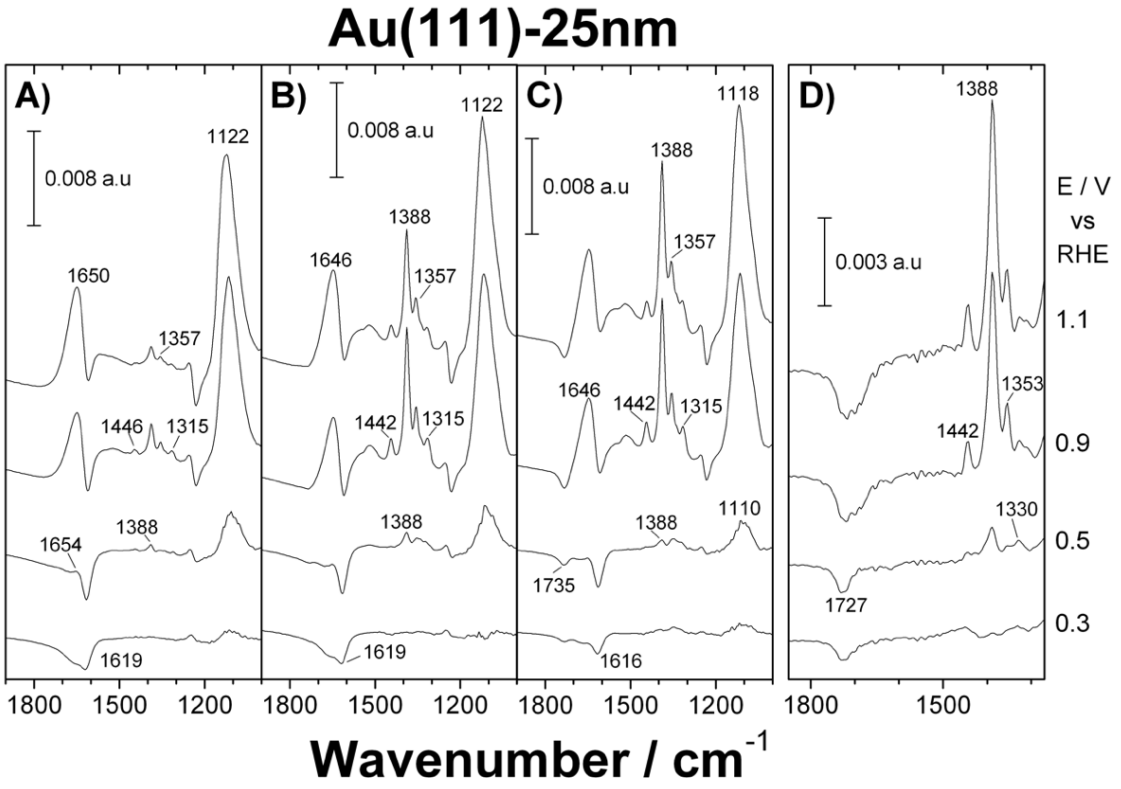

Figure 9. ATR-SEIRA spectra for an Au(111)-25nm thin film electrode in *x* mM Glu + 0.1 M $HClO_4$ (pH=1) solutions prepared in water (A-C) and D_2O (D) where *x* is 0.1 (A), 1 (B) and 10 (C and D). The spectrum obtained at 0.1V vs RHE in the same working solution was taken as the reference. 100 interferograms were collected at each potential.

The different spectra for different Glu concentrations in H_2O and D_2O are displayed in Figure 9 and the band assignment is summarized in table 1. Amino acid adsorbed bands appear between 1300-1400 cm^{-1}, corresponding to vibrational modes combining the symmetric OCO stretch of the carboxylate with bending modes involving CH_x and NH_3 groups [55]. Additionally, water bands can be detected in the O-H stretching region between 3000-4000 cm^{-1} (not shown) and O-H bending region between 1600-1700 cm^{-1}. An intense absorption band is also observed around 1100 cm^{-1}, which is related to the asymmetrical tension of the Cl-O bond in co-adsorbed perchlorate anions.

Water and perchlorate related bands have frequencies and shapes remarkably similar to those observed in amino-acid-free perchloric acid solution (figure S1-1) [56], which suggests that adsorbed glutamate species are co-adsorbed with perchlorate.

Table 1: Bands assignment in the region between 1300-1400 cm^{-1}.

Modes	ν/cm^{-1}	Refs
Sym. str. OCO + bend. CCH + bend. NH_3 + bend. CH_2 + bend. COH	1315 cm^{-1}	[57, 58]
Sym. str. OCO + bend. HCN + bend. NH_3	1357	[55]
Sym. str. OCO + bend (CCH and CH2)	1388	[55]

Two electrode potential regions can be distinguished in the spectra (Figure 9). At potentials below 0.5 V, adsorption bands are nearly absent from the spectra. However, at higher potentials, positive bands at 1315, 1357, and 1388 cm^{-1} appear, corresponding to the combined modes summarized in table 1, increasing their intensity with the electrode potential. The appearance of these bands coincides with the adsorption onset observed for glutamate.

In Figure 9C, a negative band at ca. 1730 cm^{-1} can also be observed. This band can be assigned to the carbonyl CO stretch of cationic amino acids (NH_3^+-R-**CO**OH) in solution [10, 14, 59-61]. The negative sign of the band indicates that some carboxylic groups are adsorbed at the reference potential. Since these bands appear close to the bending modes of OH in water, a better resolution can be obtained in D_2O (Figure 9D and SI-2). The spectra in deuterium oxide (Figure 9D) presents the same bands as those observed in water, though with a better defined negative band at 1720 cm^{-1}, as has been observed for carboxylic acids in D_2O [53, 55, 57, 58]. To verify that the band at 1720 cm^{-1} is related to the carboxylic groups, time-dependent ATR-SEIRA spectra were

collected for a gold thin film electrode in 10 mM glutamic acid + 0.1 M $HClO_4$ in D_2O after dosing glutamic acid (figure SI-3) at E=0.1 V. For E = 0.1 V, the Au(111) surface has a negative surface charge, promoting the interaction of the protonated amino group ($NH3^+$) with the surface. As result, the carboxylic group close to the protonated amino group (HOOC-R-$NH3^+$-COOH) presents a configuration which is not parallel to the surface, causing the vibration mode stretching ν (C = O) to be active in infrared, and the appearance of a growing positive band at 1724 cm^{-1}, which is associated with the carboxylic groups in the glutamate species. Thus, the presence of the negative band at 1720 cm^{-1} in the spectra of figure 9D clearly indicates that the carboxylic groups are being adsorbed and are involved in the adsorption process of the glutamate species, that is, carboxylic groups are in contact with the surface.

Carboxylic groups can be adsorbed in the monodentate and bidentate configuration. In the monodentate form, a band in between 1700-1500 cm^{-1}, associated with the asymmetric O-C-O stretching mode of the carboxylate group, should be expected. However, in the bidentate configuration, the dynamic dipole for the ν_{as} (OCO) mode is parallel to the electrode surface, and the corresponding band cannot be observed, as a result of the surface selection rule [59]. No bands can be observed in this region in Figure 9A-C, though they may be masked by OH related bands. The absence of these bands in D_2O (Figure 9D) unequivocally indicates that carboxylate groups are adsorbed in the bidentate configuration.

Through carboxylate groups under bidentate configuration, glutamate can be adsorbed through only one or both of these groups. To explore this end, potential-difference ATR-SEIRAS spectra scanning at 2 mV s^{-1} from 0.1 to 1.7 V in the 10 mM glutamic acid solution were obtained (Figure 10). The spectral bands at 1315, 1357, and 1388 cm^{-1} for potentials below 1.1 V are similar to those displayed in Figure 9A-C. The

1650 and 3400 cm^{-1} bands correspond to the bending and stretching modes of water molecules with strong hydrogen bonds, and the increase in the glutamate coverage by increasing the electrode potential gives rise to additional bands between 3000-2800 cm^{-1}, as seen with other amino acids (glycine) [7, 8]. These signals correspond to NH stretching when one H atom of the ammonium group is involved in a hydrogen bond with water. However, it is important to highlight that no bands are observed between 2500-2700 cm^{-1} and around 2000 cm^{-1}. These bands, which are present in the ATR-SEIRA spectra of adsorbed bioxalate [60] and bimalonate [62] on gold, are associated with hydrogen bond formation between neighbor adsorbed carboxylic groups or between these groups and water molecules [60, 62]. These short molecules cannot be adsorbed through both carboxylate groups for steric reasons, and thus, the non-adsorbed carboxylic groups can form hydrogen bonds either with water molecules or neighboring adsorbates. But the absence of these bands for longer molecules supports the proposed adsorption mode in which adsorbed glutamate is bonded to the surface through both carboxylate groups. Above 1.1 V, the signals corresponding to adsorbed glutamate disappear, indicating that glutamate is being desorbed. The absence of bands around 2170 cm^{-1}, which corresponds to the stretching of C–N bond and can be associated with the presence of adsorbed cyanide as a product of decarboxylation [16, 63], indicates that the process does not involve a breakdown of the amino acid.

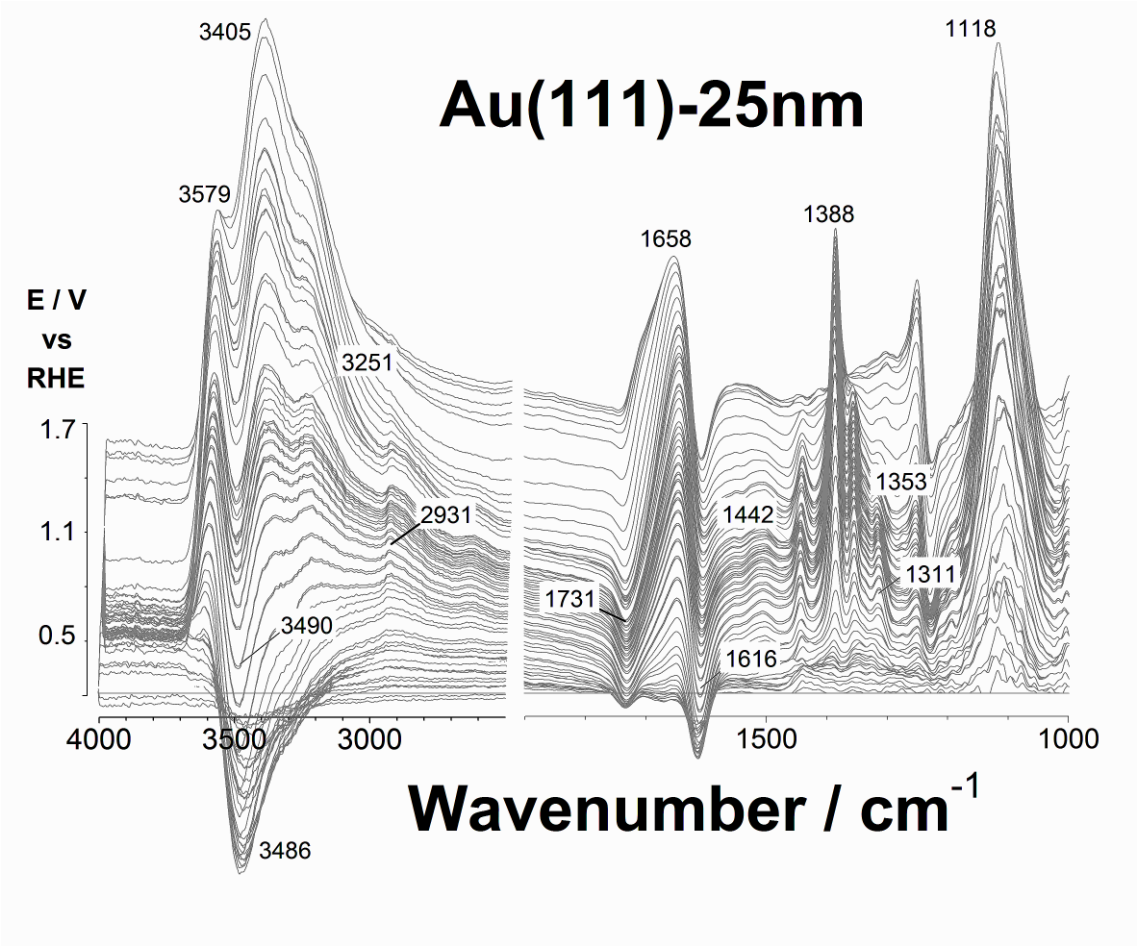

Figure 10. Potential-difference ATR-SEIRAS spectra of a potential scan for an Au(111)-25nm thin film electrode in 10 mM Glu + 0.1M $HClO_4$ in water. The spectrum at 0.1V vs RHE in the same working solution was taken as the reference, adding 104 interferograms at each potential with spectral resolution 8cm^{-1}.

3.3. DFT calculations.

Plausible configurations of glutamate species adsorbed on the Au(111) surface, with one and two dehydrogenated carboxylic groups attached to the surface in the bidentate configuration, under neutral total charge conditions, were found using DFT (Figure 11). For each relevant configuration, the free energy of the corresponding adsorption process was estimated to value plausibility. From the cationic form of Glu (protonated in the amine group), under acidic conditions, the chemisorbed state displayed in Figure 11A is favorable by 0.67 eV, which involves the bidentate attachment to the surface of the proximal carboxylic group to the amine group (the one having the lower pK_a). Later, and under less acidic conditions (higher pK_a), which favor the

dehydrogenation of the other carboxylic group, the configuration displayed in Figure 11B can be obtained, which is unfavorable only by 0.05 eV. Thus, this figure indicates that the cationic form of Glu can rest simultaneously attached to the surface through both dehydrogenated carboxylic groups in the bidentate configuration. Finally, under more alkaline conditions (the highest pK_a), the protonated amine group can be deprotonated. Figure 11C shows that a stationary chemisorbed state in which the amine group and the two dehydrogenated carboxylic groups attached to the surface, though this configuration is unfavorable by in the order of 0.55 eV. This unfavorable value can be at least in part explained by the fact that the carbon backbone of the molecule rest significantly twisted when both carboxylic groups and also the amine group are simultaneously coupled to the specific layout of the atoms exposed by the Au(111) surface.

Interestingly, for the case in which only the proximal carboxylic group to the amine group is dehydrogenated, it was found that, in the absence of dispersion forces, the bidentate attachment of the carboxylic group to the surface gives rise to a perpendicular adsorbate to the surface. Under these conditions, an unfavorable tension is originated when trying to attach the second dehydrogenated carboxylic group. However, when dispersion forces were considered, a much more horizontal adsorbate configuration was obtained (Figure 11A). This much more horizontal configuration points to a much more favorable evolution to the chemisorbed state displayed in Figure 11B. Thus, the consideration of dispersion forces is essential to computationally value these adsorption processes.

According to the calculations, the adsorption of the protonated in the amine group specie through both carboxylic groups in the bidentate configuration, under standard (ideal) conditions, would take place for $E>0.05$ eV. Considering that, from this result, it can be calculated that, under the experimental conditions, the equilibrium potential for

this adsorption process would shift ca 0.3 V, and that this value is of the order of the observed onset for this process at pH=1, it can be concluded that both experimental and computational results are mutually consistent.

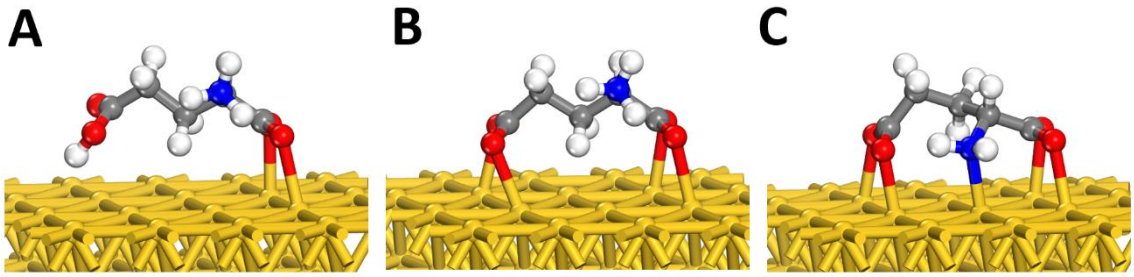

Figure 11. Adsorbed glutamate configurations on the Au(111) surface under neutral total charge conditions. With the amine group protonated (A and B) and with the protonated amine group deprotonated (C), with one (A) and two (B and C) dehydrogenated carboxylic groups attached to the surface in the bidentate configuration.

4. Conclusions.

This study demonstrates how a selected combination of electrochemical experiments, FTIR spectroscopy, and DFT calculations can be used to characterize the interaction of glutamate species with the Au(111) surface. Electrochemical experiments enable the identification of hydrogenation states, coverages, and number of electrons exchanged, spectroscopic experiments provide evidence of the presence of functional groups, and DFT calculations provide plausible adsorbent-adsorbate configurations consistent with the experiments. Electrochemical results reveal that glutamate adsorption on Au(111) requires a slightly negative potential with respect to that of the zero charge, and exchanges two electrons per adsorbed molecule. Thus, both carboxylate groups should deprotonate before adsorption, giving rise to a complex potential dependence with pH. The FTIR spectral evolution with the potential is consistent with an adsorption mode in which both carboxylate groups are bonded to the surface in a bidentate configuration (with both oxygen atoms attached to the surface). DFT calculations confirm this

adsorption mode, being the addition of dispersion forces essential to validate theoretically this interaction.

Acknowledgments.

Financial support from Ministerio de Ciencia e Innovación (Project PID2019-105653GB-100) and Generalitat Valenciana (Project PROMETEO/2020/063) is acknowledged.

References

[1] P.S. Ghosh, C. Kim, G. Han, N.S. Forbes, V.M. Rotello, Efficient Gene Delivery Vectors by Tuning the Surface Charge Density of Amino Acid-Functionalized Gold Nanoparticles., ACS Nano, 2 (2008) 2213–2218.
[2] E.C. Dreaden, A.L. Alkilany, X. Huang, C.J. Murphy, M.A. El-Sayed, The golden age: gold nanoparticles for biomedicine, Chem Soc Rev, 41 (2012) 2740–2779.
[3] D.C. Goldstein, P. Thordarson, J.R. Peterson, The Bioconjugation of Redox Proteins to Novel Electrode Materials, Australian Journal of Chemistry, 62 (2009) 1320-1327.
[4] K. Hernandez, R. Fernandez-Lafuente, Control of protein immobilization: Coupling immobilization and site-directed mutagenesis to improve biocatalyst or biosensor performance, Enzyme and Microbial Technology, 48 (2011) 107-122.
[5] R. Shukla, M. Chaudhary, A. Basu, R.R. Bhonde, M. Sastry, Biocompatibility of Gold Nanoparticles and Their Endocytotic Fate Inside the Cellular Compartment: A Microscopic Overview, Langmuir, 21 (2005) 10644–10654.
[6] D. Pedone, M. Moglianetti, E. De Luca, G. Bardi, P.P. Pompa, Platinum nanoparticles in nanobiomedicine, Chemical Society Reviews, 46 (2017) 4951-4975.
[7] O. Yamauchi, A. Odani, M. Takani, Metal–amino acid chemistry. Weak interactions and related functions of side chain groups, J. Chem. Soc. - Dalton Trans., (2002) 3411–3421.
[8] F. Huerta, E. Morallon, F. Cases, A. Rodes, J.L. Vázquez, A. Aldaz, Electrochemical behaviour of amino acids on Pt(h,k,l): A voltammetric and in situ FTIR study .1. Glycine on Pt(111), J. Electroanal. Chem., 421 (1997) 179-185.
[9] P. Lofgren, A. Krozer, J. Lausmaa, B. Kasemo, Glycine on Pt(111): A TDS and XPS study, Surf. Sci., 370 (1997) 277-292.
[10] A.P. Sandoval, J.M. Orts, A. Rodes, J.M. Feliu, Adsorption of Glycine on Au(hkl) and Gold Thin Film Electrodes: An in Situ Spectroelectrochemical Study, J. Phys. Chem. C, 115 (2011) 16439-16450.
[11] C.H. Zhen, S.G. Sun, C.J. Fan, S.P. Chen, B.W. Mao, Y.J. Fan, In situ FTIRS and EQCM studies of glycine adsorption and oxidation on Au(1 1 1) electrode in alkaline solutions, Electrochim. Acta, 49 (2004) 1249-1255.
[12] Z.-c. Zhang, J.-f. Hui, Z.-C. Liu, X. Zhang, J. Zhuang, X. Wang, Glycine-Mediated Syntheses of Pt Concave Nanocubes with High-Index {hk0} Facets and Their Enhanced Electrocatalytic Activities, Langmuir, 28 (2012) 14845-14848.

[13] L. Ruan, H. Ramezani-Dakhel, C.-Y. Chiu, E. Zhu, Y. Li, H. Heinz, Y. Huang, Tailoring Molecular Specificity Toward a Crystal Facet: a Lesson From Biorecognition Toward Pt{111}, Nano Lett., 13 (2013) 840-846.
[14] A.P. Sandoval, J.M. Orts, A. Rodes, J.M. Feliu, A comparative study of the adsorption and oxidation of L-alanine and L-serine on Au(100), Au(111) and gold thin film electrodes in acid media, Electrochim. Acta, 89 (2013) 72-83.
[15] F. Huerta, E. Morallon, J.L. Vazquez, A. Aldaz, Electrochemical behaviour of amino acids on Pt(hkl). A voltammetric and in situ FTIR study Part IV. Serine and alanine on Pt(100) and Pt(110), J. Electroanal. Chem., 475 (1999) 38-45.
[16] F. Huerta, E. Morallon, F. Cases, A. Rodes, J.L. Vázquez, A. Aldaz, Electrochemical-Behavior of Amino-Acids on Pt(H,K,L) - A Voltammetric and in-Situ FTIR Study .2. Serine and Alanine on Pt(111), J. Electroanal. Chem., 431 (1997) 269-275.
[17] G. Horanyi, A direct and indirect radiotracer study of the adsorption of serine at a platinized platinum electrode, J. Electroanal. Chem., 304 (1991) 211-217.
[18] A.P. Sandoval, J.M. Orts, A. Rodes, J.M. Feliu, DFT and In Situ Infrared Studies on Adsorption and Oxidation of Glycine, L-Alanine, and L-Serine on Gold Electrodes, in: A. Wieckowski, C. Korzeniewski, B. Braunschweig (Eds.) Wiley Ser Electrocat, John Wiley & Sons, Inc.2013, pp. 241-265.
[19] M.R. Wieckowski, C. Giorgi, M. Lebiedzinska, J. Duszynski, P. Pinton, Isolation of mitochondria-associated membranes and mitochondria from animal tissues and cells, Nat Protoc, 4 (2009) 1582-1590.
[20] J.M. Gisbert-Gonzalez, J.M. Feliu, A. Ferre-Vilaplana, E. Herrero, Why Citrate Shapes Tetrahedral and Octahedral Colloidal Platinum Nanoparticles in Water, J. Phys. Chem. C, 122 (2018) 19004-19014.
[21] J.M. Gisbert-Gonzalez, W. Cheuquepán, A. Ferré-Vilaplana, J.M. Feliu, E. Herrero, Citrate adsorption on gold: Understanding the shaping mechanism of nanoparticles, J. Electroanal. Chem., (2020) 114015.
[22] J.A. Portilla-Arias, B. Camargo, M. Garcia-Alvarez, A. Martinez de Ilarduya, S. Muñoz-Guerra, Nanoparticles Made of Microbial Poly(γ -glutamate)s for Encapsulation and Delivery of Drugs and Proteins, J. Biomater. Sci. Polym. Ed., 20 (2009) 1065–1079.
[23] K. Sonaje, Y.-J. Chen, H.-L. Chen, S.-P. Wey, J.-H. Juang, H.-N. Nguyen, C.-W. Hsu, K.-J. Lin, H.-W. Sung, Enteric-coated capsules filled with freeze-dried chitosan/poly (γ-glutamic acid) nanoparticles for oral insulin delivery., Biomaterials, 31 (2010) 3384–3394.
[24] J. Clavilier, R. Faure, G. Guinet, R. Durand, Preparation of monocrystalline Pt microelectrodes and electrochemical study of the plane surfaces cut in the direction of the {111} and {110} planes J. Electroanal. Chem., 107 (1980) 205-209.
[25] A. Rodes, E. Herrero, J.M. Feliu, A. Aldaz, Structure sensitivity of irreversibly adsorbed tin on gold single-crystal electrodes in acid media, J. Chem. Soc. Faraday T., 92 (1996) 3769-3776.
[26] J.M. Delgado, J.M. Orts, J.M. Pérez, A. Rodes, Sputtered Thin-Film Gold Electrodes for in Situ ATR-SEIRAS and SERS Studies, J. Electroanal. Chem., 617 (2008) 130-140.
[27] B. Delley, An all-electron numerical method for solving the local density functional for polyatomic molecules, J. Chem. Phys., 92 (1990) 508-517.
[28] B. Delley, Hardness conserving semilocal pseudopotentials, Phys. Rev. B, 66 (2002) 155125.
[29] B. Hammer, L.B. Hansen, J.K. Nørskov, Improved adsorption energetics within density-functional theory using revised Perdew-Burke-Ernzerhof functionals, Phys. Rev. B, 59 (1999) 7413-7421.

[30] B. Delley, From molecules to solids with the DMol(3) approach, J. Chem. Phys., 113 (2000) 7756-7764.
[31] A. Tkatchenko, M. Scheffler, Accurate Molecular Van Der Waals Interactions from Ground-State Electron Density and Free-Atom Reference Data, Phys. Rev. Lett., 102 (2009) 073005.
[32] B. Delley, The conductor-like screening model for polymers and surfaces, Mol. Simulat., 32 (2006) 117-123.
[33] J. Neugebauer, M. Scheffler, Adsorbate-substrate and adsorbate-adsorbate interactions of Na and K adlayers on Al(111), Phys. Rev. B, 46 (1992) 16067-16080.
[34] J.K. Nørskov, J. Rossmeisl, A. Logadottir, L. Lindqvist, J.R. Kitchin, T. Bligaard, H. Jónsson, Origin of the Overpotential for Oxygen Reduction at a Fuel-Cell Cathode, J. Phys. Chem. B, 108 (2004) 17886-17892.
[35] H. Angersteinkozlowska, B.E. Conway, A. Hamelin, L. Stoicoviciu, Elementary Steps of Electrochemical Oxidation of Single-Crystal Planes of Au .2. A Chemical and Structural Basis of Oxidation of the (111) Plane, J. Electroanal. Chem., 228 (1987) 429-453.
[36] H. Angerstein-Kozlowska, B.E. Conway, A. Hamelin, L. Stoicoviciu, Elementary Steps of Electrochemical Oxidation of Single-Crystal Planes of Au .1. Chemical Basis of Processes Involving Geometry of Anions and the Electrode Surfaces, Electrochim. Acta, 31 (1986) 1051-1061.
[37] A. Hamelin, The crystallographic orientation of gold surfaces at the gold-aqueous solution interphaces, J. Electroanal. Chem., 142 (1982) 299.
[38] S. Strbac, A. Hamelin, R.R. Adzic, Electrochemical indication of surface reconstruction of (100), (311) and (111) gold faces in alkaline solutions, J. Electroanal. Chem., 362 (1993) 47-53.
[39] A. Hamelin, M.J. Sottomayor, F. Silva, S.C. Chang, M.J. Weaver, Cyclic Voltammetric Characterization of Oriented Monocrystalline Gold Surfaces in Aqueous Alkaline-Solution, J. Electroanal. Chem., 295 (1990) 291-300.
[40] U. Harten, A.M. Lahee, J.P. Toennies, C. Wöll, Observation of a soliton reconstruction of au(111) by high-resolution helium-atom diffraction, Phys. Rev. Lett., 54 (1985) 2619-2622.
[41] S. Narasimhan, D. Vanderbilt, Elastic stress domains and the herringbone reconstruction on au(111)
Phys. Rev. Lett., 69 (1992) 1564-1567.
[42] X. Gao, A. Hamelin, M.J. Weaver, Atomic relaxation at ordered electrode surfaces probed by sanning tunneling microscopy : Au(111) in aqueus solution compared with ultrahigh-vacuum enviroments, J. Chem. Phys., 95 (1991) 6993-6996.
[43] D.M. Kolb, Reconstruction phenomena at metal-electrolyte interfaces, Prog. Surf. Sci., 51 (1996) 109-173.
[44] X. Gao, S.C. Chang, X. Jiang, A. Hamelin, M.J. Weaver, Emergence of atomic level structural information for oredered metal-solution interfaces : some recent contributions from in- situ infrared spectroscopy and scanning tunneling microscopy, J. Vac. Sci. Technol. A, 10 (1992) 2972.
[45] A. Sadkowski, A.J. Motheo, R.S. Neves, Characterisation of au(111) and au(210) aqueous solution interfaces by electrochemical immittance spectroscopy, J. Electroanal. Chem., 455 (1998) 107-119.
[46] U.W. Hamm, D. Kramer, R.S. Zhai, D.M. Kolb, The pzc of Au(111) and Pt(111) in a perchloric acid solution: An ex situ approach to the immersion technique, J. Electroanal. Chem., 414 (1996) 85-89.

[47] A. Hamelin, Cyclic voltammetry at gold single-crystal surfaces .1. Behaviour at low-index faces, J. Electroanal. Chem., 407 (1996) 1-11.
[48] A. Hamelin, Note on the behavior of the (111) gold face in electrolytic solutions, J. Electroanal. Chem., 210 (1986) 303-309.
[49] D.M. Kolb, J. Schneider, Surface reconstuction in electrochemistry: Au(100)-(5x20), Au(111)-(1x23) and Au(110)-(1x2), Electrochim. Acta, 31 (1986) 929-936.
[50] A. Hamelin, Study of the (210) face of gold in aqueous solutions, J. Electroanal. Chem., 138 (1982) 395-400.
[51] R.J. Nichols, I. Burgess, K.L. Young, V. Zamlynny, J. Lipkowski, A quantitative evaluation of the adsorption of citrate on Au(111) using SNIFTIRS, J. Electroanal. Chem., 563 (2004) 33-39.
[52] R.P. S. Trasatti, Interphases in Systems of Conducting Phases, J. Electroanal. Chem., 205 (1986) 359-376.
[53] M. Osawa, Surface-Enhanced Infrared Absorption Spectroscopy, Handbook of Vibrational Spectroscopy, John Wiley & Sons, Ltd2006.
[54] R. Aroca, Surface enhanced vibrational spectroscopy, John Wiley & Sons Ltd, Chichester (UK), 2006.
[55] A. Wieckowski, C. Korzeniewski, B. Braunschweig, Vibrational Spectroscopy at Electrified Interfaces, 1 ed., Wiley2013.
[56] K. Ataka, T. Yotsuyanagi, M. Osawa, Potential-dependent reorientation of water molecules at an electrode/electrolyte interface studied by surface-enhanced infrared absorption spectroscopy, J. Phys. Chem., 100 (1996) 10664-10672.
[57] S.E. Cabaniss, I.F. McVey, Aqueous infrared carboxylate absorbances: aliphatic monocarboxylates, Spectrochim. Acta A, 51 (1995) 2385-2395.
[58] S.E. Cabaniss, J.A. Leenheer, I.F. McVey, Aqueous infrared carboxylate absorbances: aliphatic di-acids, Spectrochim. Acta A, 54 (1998) 449-458.
[59] R.G. Greenler, Infrared Study of Adsorbed Molecules on Metal Surfaces by Reflection Techniques, J. Chem. Phys., 44 (1966) 310-315.
[60] A. Berna, J.M. Delgado, J.M. Orts, A. Rodes, J.M. Feliu, In-situ infrared study of the adsorption and oxidation of oxalic acid at single-crystal and thin-film gold electrodes: A combined external reflection infrared and ATR-SEIRAS approach, Langmuir, 22 (2006) 7192-7202.
[61] G. Socrates, Infrared and Raman characteristic group frequencies: tables and charts, Wiley2001.
[62] J.M. Delgado, A. Berna, J.M. Orts, A. Rodes, J.M. Feliu, In situ infrared study of the adsorption and surface acid-base properties of the anions of dicarboxylic acids at gold single crystal and thin-film electrodes, J. Phys. Chem. C, 111 (2007) 9943-9952.
[63] Y.-J. Gu, S.-G. Sun, S.-P. Chen, C.-H. Zhen, Z.-Y. Zhou, Adsorption of Serine on Pt Single-Crystal Electrodes in Sulfuric Acid Solutions, Langmuir, 19 (2003) 9823-9830.